Journal of Colloid and Interface Science 708 (2026) 139798

Contents lists available at ScienceDirect

Journal of Colloid And Interface Science

journal homepage: www.elsevier.com/locate/jcis

Structural determinants underlying the supramolecular binding between carborane and proteins in water

Tainah Dorina Marforio [a,b,1], Andrea Carboni [a,1], Luca Mazzei [c,1], Sara Cascone [a], Lorenzo Lovatti [a], Edoardo Jun Mattioli [a,b], Francesco Valle [d,e], Matteo Di Giosia [a,b], Stefano Ciurli [c,*], Matteo Calvaresi [a,b,**]

[a] Dipartimento di Chimica 'Giacomo Ciamician', Alma Mater Studiorum – Università di Bologna, Via Gobetti 85, 40129 Bologna, Italy
[b] IRCCS Azienda Ospedaliero – Universitaria di Bologna, Preclinical & Translational Research in Oncology Lab (PRO), Bologna, Italy
[c] Laboratorio di Chimica Bioinorganica, Dipartimento di Farmacia e Biotecnologie, Alma Mater Studiorum - Università di Bologna, 40127 Bologna, Italy
[d] Istituto per lo Studio dei Materiali Nanostrutturati, Consiglio Nazionale delle Ricerche, 40129 Bologna, Italy
[e] CSGI, Consorzio Sistemi a Grande Interfase, University of Florence, Sesto Fiorentino, Italy

GRAPHICAL ABSTRACT

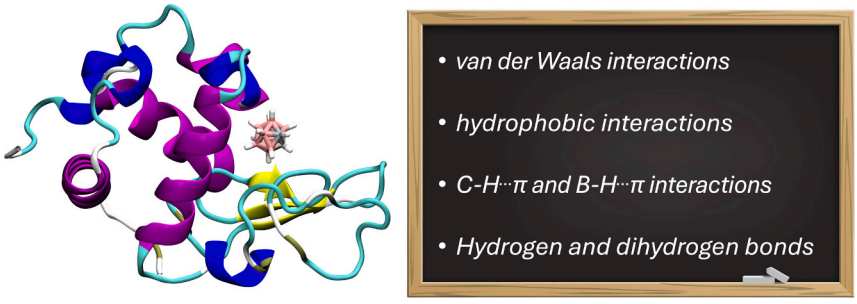

ARTICLE INFO

Keywords:
Carborane-protein interactions
Supramolecular binding
Hydrophobic interactions
Boron neutron capture therapy
Molecular dynamics simulations

ABSTRACT

Carboranes are chemically and biologically stable boron-carbon clusters with promising applications in medicinal chemistry. While their use in boron neutron capture therapy (BNCT) has been extensively explored, recent attention has shifted toward understanding their interactions with biological macromolecules, particularly proteins. Here, we characterize the interaction between *closo*-ortho-carborane and lysozyme (LSZ) using NMR spectroscopy, molecular docking and molecular dynamics simulations, and enzymatic assays. Experimental data demonstrate that carborane forms a stable 1:1 complex with LSZ (Carborane@LSZ), retaining the monomeric state and the protein fold, with only a limited number of amino acids involved in the interaction. In particular, NMR chemical shift perturbations revealed specific binding near the substrate-binding pocket, a result corroborated by molecular docking and molecular dynamic simulations. Carborane fits into a hydrophobic pocket near the substrate-binding site, where the recognition process is driven by hydrophobic interactions complemented by classical hydrogen and non-standard dihydrogen bonding. Carborane-@LSZ complex partially inhibits enzymatic

* Corresponding author at: Dipartimento di Farmacia e Biotecnologie, Alma Mater Studiorum - Università di Bologna, Via Fanin 40, 40127 Bologna, Italy.
** Corresponding author at: Dipartimento di Chimica 'Giacomo Ciamician', Alma Mater Studiorum – Università di Bologna, Via Gobetti 85, 40129 Bologna, Italy.
E-mail addresses: stefano.ciurli@unibo.it (S. Ciurli), matteo.calvaresi3@unibo.it (M. Calvaresi).
[1] These authors equally contributed to this work

https://doi.org/10.1016/j.jcis.2025.139798
Received 3 July 2025; Received in revised form 18 December 2025; Accepted 26 December 2025
Available online 27 December 2025

activity (~33 %). Extending this approach to bovine serum albumin (BSA) revealed similar binding principles, underscoring the generality of carborane–protein supramolecular interactions. These findings provide fundamental insights into pristine carboranes recognition by proteins and establish a foundation for designing carborane-based therapeutics and delivery platforms in nanomedicine.

1. Introduction

Carboranes are a class of boron-carbon-hydrogen clusters with unique structural and chemical properties, with the icosahedral "*closo*-carboranes" being the most common member of the family [1,2]. These clusters are characterized by their high aromaticity, hydrophobicity and consequent lipophilic nature, as well as high chemical and thermal stability. Such properties render carboranes attractive scaffolds in medicinal chemistry, as their abiotic nature, manifested by resistance to metabolic degradation and kinetic inertness, offers clear advantages over more traditional organic moieties [1–9].

The medicinal chemistry of carboranes has traditionally focused on their use in boron neutron capture therapy (BNCT).[10] In BNCT, ^{10}B-containing compounds are selectively delivered to cancer cells; upon irradiation with low-energy neutrons, the ^{10}B atoms undergo a nuclear fission that generates ^{7}Li together with high-energy α-particles and γ-rays capable of destroying the targeted tumour cells with minimal damage to surrounding healthy tissues. Carboranes are particularly well suited for BNCT because of their high boron content, chemical stability, and low toxicity.

Carboranes possess several pharmacophoric features, such as hydrophobicity, aromaticity, and the ability to act as both hydrogen bonding donors and acceptors. Their structural rigidity is particularly advantageous for the development of protein inhibitors as it decreases the binding entropic penalty. These properties enable carboranes to expand the chemical space available for drug development [1–10].

Structurally, carboranes are isosteric with phenyl rings, and replacing aromatic groups with carborane cages often enhances drug potency by promoting stronger hydrophobic and dispersion-driven interactions [11,12], especially in proteins with concave, nonpolar aromatic binding sites [8]. Consequently, carborane-containing compounds have been successfully applied in therapeutic strategies targeting cancers, infectious diseases, and neurodegenerative disorders [1–11,13–41]. Recently, owing to their rigidity and hydrophobicity, carboranes have also been employed as hydrophobic tags for the degradation of various proteins [42].

The spherical polyhedral structure of carboranes allows them to fits snugly within protein cavities and concave binding pockets [1–10,13], thereby maximizing hydrophobic interactions. In addition, carboranes can interact strongly with aromatic residues *via* C–H···π and B–H···π interactions [11,12]. Beyond forming classical hydrogen bonds through their acidic C—H protons, carboranes are also capable of establishing dihydrogen bonds [43,44], wherein their hydridic B—H groups interact with hydrogen-bond donors in proteins, further expanding their repertoire of molecular interactions.

In addition to their use in drug development, the interaction of carboranes with proteins can be exploited to improve their application in BNCT. In this context, proteins can serve as "Trojan horses" [45–47], facilitating the supramolecular dispersion of carboranes in physiological environments through host-guest interactions and enabling the targeted delivery of high boron concentrations to specific cells or tissues. This supramolecular strategy offers both structural and functional advantages for targeted delivery, imaging, and multimodal cancer therapy [48–50].

To date, studies investigating the interactions of carboranes with proteins have primarily relied on crystal structures and functionalized carborane derivatives [11,14–26], in which chemical pendants of the cluster typically dictate the binding to the protein. However, a comprehensive understanding of the binding interaction between non-functionalized carborane clusters and proteins in aqueous solutions remains incomplete.

In this study, we address this knowledge gap by using hen egg-white lysozyme (LSZ) as a model protein. LSZ is an ideal choice due to its small size (~14 kDa), high solubility in aqueous media, and consequent suitability for high-resolution NMR characterization under aqueous conditions, an approach generally not feasible for larger proteins. Here, we elucidate the binding mode and interaction dynamics of LSZ with pristine *closo*-ortho-carborane in aqueous solution by combining NMR chemical shift perturbation (CSP) analysis with computational modelling. To further validate our methodology, we also examined a second model protein, bovine serum albumin (BSA). The results of this study provide new insights into the interaction properties of a carborane-protein complexes in a biologically relevant environment.

2. Materials and methods

Synthesis of the OCB@protein complex.

A 1 mL solution of lysozyme (Sigma-Aldrich, code L6876) at a concentration of 1 mM in milli-Q water was gently added into a 2 mL Eppendorf containing approximately 1.5 mg of ortho-carborane (98 %, Thermo Scientific, code 35131).The samples were placed in an ice bath and sonication was performed with a probe tip sonicator (UP200St, 200 W; Hielscher Ultrasonics) for 1 h at 32 % amplitude, resulting in a white milky suspension. The samples were then centrifuged at 10,000 rpm for 10 min; the obtained clear supernatants were collected and stored in the dark at 3–5 °C until further use. The same approach was used for bovine serum albumin (Sigma-Aldrich, code A7030).

Characterization of the OCB@lysozyme complex.

Fast Protein Liquid Chromatography analysis. Fast Protein Liquid Chromatography (FPLC) analysis was carried out using an AKTA pure system (GE Healthcare) equipped with a size exclusion chromatography Superose 6 increase 10–300 GL column (GE Healthcare). The chromatography was carried out using a flow rate of 0.5 mL/min with an elution buffer of 50 mM sodium phosphate, 150 mM NaCl, pH 7.0 and injection volume of 120 µL. The UV detector was set at 280 nm.

UV–Vis spectroscopy analysis. UV–vis absorption spectra of proteins were recorded at 25 °C by means of an Agilent Cary 60 UV–Vis spectrophotometer.

Microwave plasma atomic emission spectroscopy analysis. Analysis of the boron content was performed following a previously reported protocol [51]. Briefly, 0.4 mL of each sample was transferred in a tube subsequently filled with reagent grade HNO_3 (1.5 mL, 65 %; Sigma-Aldrich), H_3PO_4 (0.5 mL, 85 %; Sigma-Aldrich) and H_2O_2 (0.5 mL, 30 %; Sigma-Aldrich) and acid digestion was carried out at 80 °C for 8 h. The samples were diluted with milli-Q water before undergoing elemental analysis with microwave plasma atomic emission spectroscopy (4210 MP-AES, Agilent Technologies). The samples were injected at a flow rate of 0.4 mL/min and the boron was detected by monitoring the emission at 249.772 nm. Quantitation was achieved with external calibration in the 0.2–50 mg/L range, obtained from the dilution of a 1 g/L boric acid commercial standard. Nitric acids blanks were run between each sample to monitor the boron carry over in the instrument during the analysis and when needed a solution of acidified NaF at 0.6 mg/mL was run to decrease the boron memory effect according to a preusly reported procedure [52].

Atomic force microscopy analysis. AFM images were performed by a Multimode VIII equipped with a Nanoscope V (Bruker AFM, Santa Barbara, CA, US) controller and operated in ScanAsyst mode. Images

were collected at a 1 line per second scan rate with ScanAsyst Fluid+ cantilevers (nominal spring constant k = 0.7 N/m). The samples were prepared as reported previously [53]; briefly 10 μL of the final dilutions (100 x and 1000 x) of the stock solution were spotted onto freshly cleaved mica and left 10 min at room temperature to adsorb. The samples were then plugged in the AFM imaging cell avoiding any drying and imaged in milliQ water. Profile analysis of the AFM images was determined using Gwyddion.

Nuclear Magnetic Resonance analysis. NMR experiments were conducted on 3.0 mM samples of unlabeled LSZ or the corresponding Carborane@LSZ complex, prepared as described above, in 90/10 % H_2O/D_2O at pH 3.8. The HSQCFPF3GPPHWG sequence was used to acquire ^{1}H,^{15}N-edited natural abundance HSQC spectra on a Bruker Avance 900 spectrometer operating at the proton nominal frequency of 899.78 MHz (21.1 T) and equipped with a 5-mm TCI-HCN z-gradient cryo-probe. The temperature was maintained at 308 K. ^{1}H chemical shifts were referenced to 2,2-dimethyl-2-silapentane-5-sulfonic acid sodium salt (DSS), while ^{15}N chemical shifts were referenced indirectly to DSS using the ratios of the gyromagnetic constants. The ^{1}H,^{15}N HSQC spectra were acquired with a total of 512 transients, spectral widths of 14,705.882 Hz (^{1}H, 16.3 ppm cantered at 4.701 ppm) and 3649.635 Hz (^{15}N, 40.0 ppm, cantered at 118 ppm), and maximal evolution times of 69.6 ms (^{1}H, 2048 points) and 19.2 ms (^{15}N, 140 t_1 increments in States-TPPI mode detection). The sequence was optimized with an INEPT delay $1/(4J_{NH})$ of 2.78 ms (J_{NH} = 90 Hz). A recycle delay of 1.0 s was used, and decoupling during the acquisition time was achieved using a GARP4 scheme.

All NMR spectra were processed using NMRpipe [54]. The raw data were zero-filled to 2048 × 1024 points, a cosine-squared apodization function was applied in both dimensions, and the SMILE algorithm [55] was used for processing the 2D NMR spectra after Fourier transformation.

Peak peaking and spectral analysis were carried out using POKY [56]. Resonance assignments for LSZ were based on the available chemical shifts (BMRB Entry 4831). Chemical shift changes upon complex formation with Carborane were reported as weighted average chemical shift differences $\Delta\delta_{avg}$(HN) to account for differences in spectral widths between ^{1}H and ^{15}N resonances. $\Delta\delta_{avg}$(HN) values were calculated as $\Delta\delta_{avg}(HN) = [(\Delta\delta_H\ [2] + (\Delta\delta_N/7)\ [2])]^{1/2}$ (or $\Delta\delta_{avg}(HN) = [(\Delta\delta_H\ [2] + (\Delta\delta_N/5)\ [2])]^{1/2}$ for glycines [57,58], where $\Delta\delta_H$ and $\Delta\delta_N$ are the chemical shift differences for ^{1}H and ^{15}N, respectively.

Enzymatic activity tests. The activity of the lysozyme was measured *via* turbidity-based activity assay [59], *i.e.* by monitoring the enzymatic degradation of a bacterial substrate suspension. A 0.015 % [w/v] stock solution of *Micrococcus lysodeikticus* (ATCC No. 4698, lyophilized cells; Sigma-Aldrich) was prepared in phosphate buffer at pH 6.2. Aliquots of the protein samples at 300 units/mL were added according to the producer's instruction and the UV absorbance at 450 nm (A_{450}) was monitored over time. The UV–vis spectra for the enzymatic activity test were collected with a Cary 60 UV–vis Spectrophotometer (Agilent Technologies).Lysozyme activity was measured by monitoring the release of 4-methylumbelliferone from the substrate 4-methylumbelliferyl β-D-*N*,*N*′,*N*′-triacetylchitotrioside hydrate ($(NAG)_3$-MUF; Sigma-Aldrich, code M5639). A 100 μM stock solution of $(NAG)_3$-MUF was prepared in an 80:20 H_2O:DMSO mixture. Sample solutions were prepared in 0.5 mL ammonium acetate buffer (25 mM, pH 4.6) by mixing 5 μL of the enzyme with increasing concentrations of $(NAG)_3$-MUF in the 1–30 μM range. The incubation was carried out at 42 °C for 30 min and stopped by adding 60 μL of 1M NaOH. The released 4-methylumbelliferone was quantified by fluorescence emission spectroscopy using an excitation wavelength of 360 nm and detecting emission at 455 nm (EnSpire, PerkinElmer).

Computational Methods

Docking. Ortho-carborane was docked to LSZ (PDB ID = 1HEW) [60] and BSA (PDB ID = 4F5S) [61] crystallographic structures using Patchdock [62].

MM refinement. Carborane, adamantane and benzene were modelled using GAFF (General Amber Force Field) [63]. For the carborane, the previously developed *ad hoc* parameters were used [64]. LSZ and BSA were described using the FF14SB force field implemented in the Amber16 [65]. Each docking pose was optimized to relax the structure and remove steric clashes by 500 steps of steepest descend and additional 500 conjugate gradient steps of minimization. Subsequently, MM-GBSA calculations were performed on the minimized structures to obtain a ranking of the carborane@LSZ and carborane@BSA interactions, providing a more accurate assessment than the initial docking scoring function.

MD simulation. The carborane@LSZ and carborane@BSA complexes showing the largest binding energy were solvated using explicit water molecules (TIP3P) and the total charge of the systems was neutralized adding counterions. Periodic boundary conditions (PBC) and Particle Mesh Ewald (PME) with a cut-off radius of 8.0 Å were imposed. The systems were equilibrated through i) an initial heating from 0 to 298 K under constant volume (NVT), using Langevin dynamics and SHAKE to constrain bonds involving hydrogens, ii) a switch to NPT for pressure equilibration at 298 K, and iii) additional Langevin dynamics (NPT) to allow the system density to fully relax. After equilibration, 500 ns MD simulations were performed under isothermal-isobaric (NPT) conditions at 298 K and 1 atm, along with SHAKE constraints on hydrogen atoms.

Molecular Mechanics – Generalized Born Surface Area (MM-GBSA) calculations. The scoring of the docking poses and the calculation of the interaction between the carborane and LSZ or BSA during the MD simulation were obtained using CPPTRAJ [66]. 1000 snapshots were extracted from the MD trajectory and binding energy calculations were performed using the MMPBSA.py tool implemented in Amber16. Polar solvation energies were evaluated using the GBHCT model (*i.e.* igb = 1) [67,68] while the non-polar solvation term was computed based on the solvent-accessible surface area (SASA). Energy decomposition analysis on a per-residue basis was carried out to identify key residues contributing most significantly to ligand binding.

Trajectory analysis. CPPTRAJ tool [66] was used to perform the hydrogen and di-hydrogen bonds analysis on the trajectory.

QM/MM Calculations. Following the ONIOM approach [69,70], as implemented in Gaussian16 [71], the carborane@LSZ system was divided into two regions: a high-level (HL) region consisting of the carborane molecule and the residues forming lysozyme binding pocket (Glu35, Asp52, Leu56, Gln57, Ile58, Asn59, Trp62, Trp63, Ile98, Asn103, Ala107, Trp108, Val109, and Arg112), and a low-level (LL) region comprising the remainder of the protein. Link atoms [72] were introduced to cap the dangling bonds at the HL/LL boundary, and the electrostatic embedding scheme was used to account for inter-region interactions. The HL region was treated using density functional theory (DFT) with the ωB97X-D functional and the 6-31G* basis set, whereas the LL region was described using amber FF14SB. A set of 10 representative frames was extracted from the MD simulation of carborane@LSZ and subjected to full geometry optimization using the QM/MM protocol described above to compute the binding energy between carborane and lysozyme.

3. Results and discussion

To overcome the intrinsic hydrophobicity and aqueous insolubility of carborane, we employed a hetero-phase synthetic method assisted by ultrasonication. Proteins can be used as supramolecular hosts for carborane due to the presence of a non-polar cavities that are appropriately sized to accommodate the carborane cage, a recognition mechanism governed by concave–convex complementarity, and a high degree of binding-pocket preorganization, which minimizes the entropic penalty associated with guest binding. Ultrasonication transiently disperses the carborane into monomolecular units that can be captured in water by the proteins. Once the external stimulus ceases, the bound species fall into a kinetic trap, thereby yielding a stable adduct. Lysozyme already

demonstrated the ability to disperse in water hydrophobic molecules and nanoparticles such as fullerenes [73–75] and carbon nanotubes [76]. Briefly, LSZ dissolved in Milli-Q water was mixed with an excess of carborane powder (10:1 carborane:lysozyme molar ratio). The suspension was subjected to probe-tip ultrasonication for 60 min, resulting in the dispersion of carborane into the protein solution. The resulting mixture was centrifuged to remove insoluble aggregates, and the supernatant, containing the solubilized carborane-lysozyme adduct, was collected for analysis. The concentration of the carborane@LSZ complex was determined using UV–visible spectroscopy (Fig. S1A), while the carborane content was determined by measuring boron levels using microwave plasma atomic emission spectroscopy (MP-AES) (Fig. S1B). The resulting molar ratio of carborane to lysozyme was 1.14 ± 0.31, consistent with the formation of a stable 1:1 carborane@LSZ complex.

Size exclusion chromatography (Fig. 1A) indicated that the carborane@LSZ adduct is monomeric, thus excluding the formation of aggregates.

Atomic force microscopy (AFM) provided direct evidence of the carborane@LSZ dispersion at the nanoscale. AFM imaging revealed that the carborane@LSZ hybrids were uniformly and monomolecularly distributed across the mica surface (Fig. 1B). Height distribution analysis (Fig. 1C) further confirmed the absence of aggregates or carborane nanoparticles, supporting the formation of discrete, singly adsorbed carborane@LSZ complexes. These observations are consistent with a well-dispersed, non-aggregated hybrid system.

To assess the structural changes induced by carborane binding to LSZ at the atomic level, ^{1}H,^{15}N HSQC NMR spectra of samples of free LSZ and carborane@LSZ were analysed and the chemical shift perturbations (CSP) of backbone amide ^{1}H and ^{15}N nuclei were determined. NMR spectroscopy represents a useful tool in nanomedicine to study the interaction between ions [77], molecules [73,74], nanoparticles [78,79] and proteins.

Fig. 2A shows the ^{1}H,^{15}N HSQC spectrum of free LSZ, in which each cross-peak corresponds to a backbone NH group; in the spectrum, proline residues are not visible because they lack the backbone NH moiety, while the N-terminal NH_3^+ group is not detected due to rapid proton exchange with water that shifts its signal under the large water envelope. In addition to backbone NH signals, the spectrum also includes signals from the indole NH group of six tryptophan residues, appearing in the 9–11 ppm ^{1}H region, as well as twin cross-peaks from the side-chain NH_2 groups of asparagine and glutamine, located in the 105–112 ppm ^{15}N region. A comparison with the ^{1}H,^{15}N HSQC spectrum of the carborane@LSZ complex reveals the same high spectral resolution and very similar positions of the NH signals, indicating that the overall fold of the protein remains intact upon complex formation. Indeed, small CSP values (Fig. 2B) are observed for most residues, suggesting the absence of major conformational changes. However, a limited number of backbone NH groups exhibit significant chemical shift deviations, consistent with a localized and specific interaction between carborane and discrete regions of the LSZ surface.

Notably, the residues exhibiting the largest chemical shift changes are Phe34, Thr51 and Thr69, which are located within a specific region of the protein (Fig. 2A and 2B), surrounding the active site. Docking calculations (Fig. 2C) identify the same region as the most probable carborane binding site, which is fully accessible for supramolecular complex formation. All the possible geometries of interaction between carborane and lysozyme were identified and scored by MM-GBSA calculations (Fig. S2). In the most interacting pose, carborane is positioned in the substrate binding pocket of the enzyme, in a cleft that separates the α (residues 1–35 and 85–129) and β domains (residues 36–84) of LSZ, in close contact with the residues identified by NMR. Using the program CAVER [80], we mapped the protein tunnels (Fig. S3) to determine the accessible pathways that allow the carborane to reach its binding site from the solvent. The calculation clearly identified the accessibility of the binding site for the carborane.

The NMR analysis is limited to perturbations of backbone amide NH signals, primarily reflecting changes in the protein secondary and tertiary structure. Consequently, the possibility that other amino acids can bind the carborane through their side chains cannot be excluded. To explore these potential interactions at atomic resolution, a 500-ns molecular dynamics (MD) simulation to investigate the behaviour of the carborane cage in complex with lysozyme was carried out.

The analysis of the secondary structure of the protein in the carborane@LSZ adduct showed that during the MD simulations the secondary and tertiary structures of the lysozyme were practically unaffected by the interaction with the carborane (Fig. S4), as also observed by NMR. The carborane is blocked between the rigid secondary structures of the α and β domains, in a pre-formed hydrophobic cavity, and the rearrangement of the protein is limited (Fig. 2C).

A Molecular Mechanics–Generalized Born Surface Area (MM–GBSA) analysis of the trajectories was performed to estimate the binding energy ($E_{binding}$) that is −16.8 kcal mol^{-1} (Fig. 3A). The analysis of the energetic terms of the binding energy (Fig. 3A) between lysozyme and carborane allows the identification of the thermodynamics contributions that govern the binding of carboranes to proteins and supply guidelines of general applicability to understand their interactions.

The driving force of the binding between carborane and lysozyme is represented by the van der Waals term (E_{VDW} = −18.1 kcal mol^{-1}). It is important to highlight that in the MM-GBSA model this term considers also dispersion interactions, such as C–H···π and B–H···π interactions [11,12], that are crucial for the binding of the carborane cage to the protein. Due to its hydrophobic nature, the non-polar solvation term, *i.e.* hydrophobic effect, also promotes the binding of the carborane to the proteins (E_{surf} = −2.6 kcal mol^{-1}), although this contribution is much smaller than E_{vdW}. The existing surface complementarity between the carborane cage and the lysozyme binding pocket, that is a rapid way to estimate the stabilizing van der Waals and hydrophobic interactions, is clear in Fig. 3B.

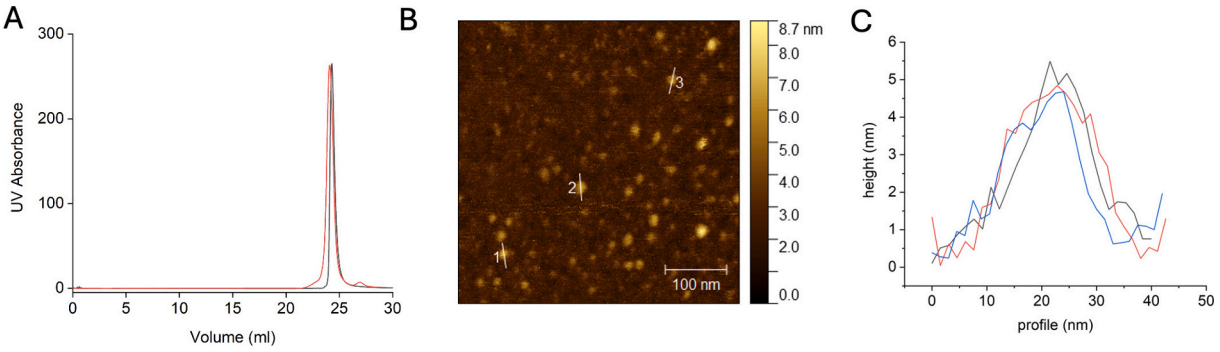

Fig. 1. A) Size exclusion chromatography of LSZ (black line) and carborane@LSZ (red line). B) AFM image of carborane@LSZ, top view (500 nm × 500 nm); scale bar: 100 nm. C) Representative profile analysis of the AFM image: profile 1 (black line), profile 2 (red line) and profile 3 (blue line) in Fig. 1B. (For interpretation of the references to colour in this figure legend, the reader is referred to the web version of this article.)

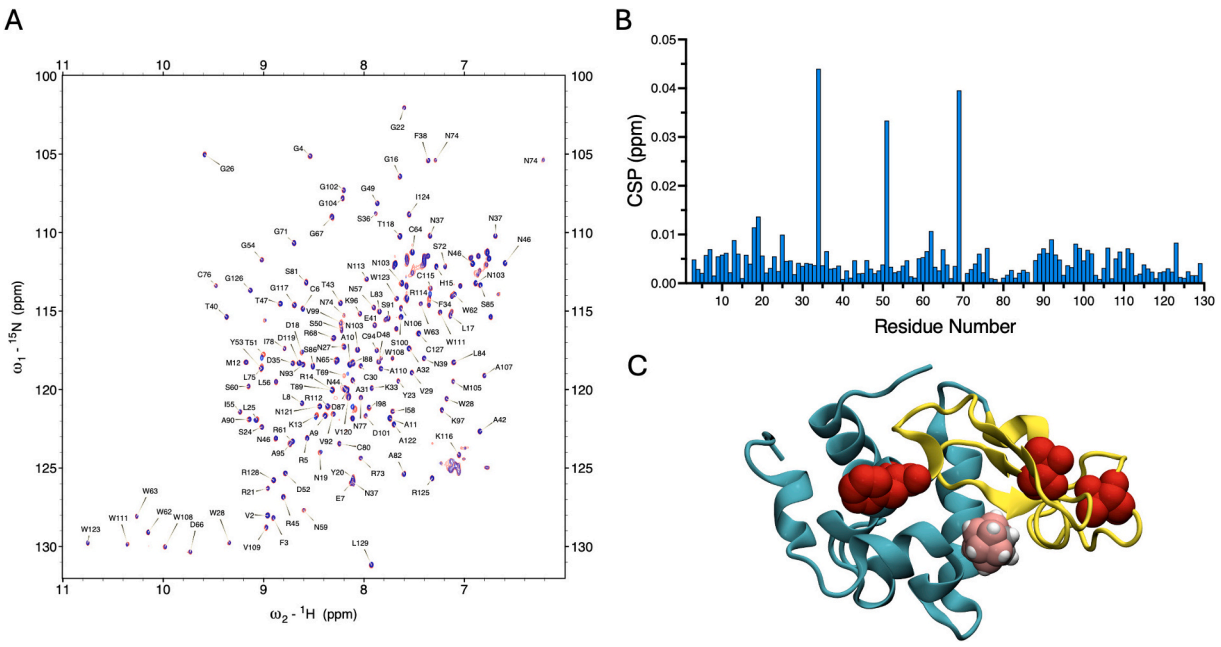

Fig. 2. NMR chemical shift perturbation (CSP) analysis of LSZ upon interaction with carborane. A) Superposition of ^{1}H,^{15}N HSQC spectra of samples of free LSZ (blue) and carborane@LSZ hybrid (red). Black labels indicate cross-peak assignment of amino acid residues. B) CSP is given by the weighted average chemical shift differences $\Delta\delta_{avg}$(HN) of cross-peaks in the ^{1}H,^{15}N HSQC spectra of free and bound LSZ. C) Docking of carborane in the LSZ structure (light blue: α domain, yellow: β domain). In red the residues undergoing major chemical shift changes upon carborane binding. (For interpretation of the references to colour in this figure legend, the reader is referred to the web version of this article.)

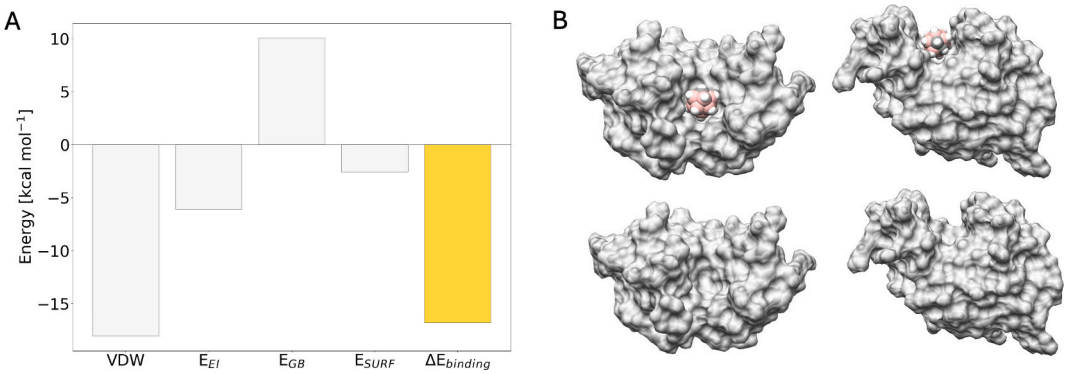

Fig. 3. A) Energy components of $E_{binding}$. B) Surface complementarity between the protein and the carborane cage. Top view and front view.

Electrostatic interactions (E_{el}), that in the MM-GBSA model also include the formation of hydrogen/dihydrogen bonds, account for −6.1 kcal mol^{-1} and are stabilizing. The only term that is detrimental to the binding is polar solvation (E_{GB} = 10.0 kcal mol^{-1}). Carborane is hydrophobic, but its binding occurs in the substrate binding pocket of the lysozyme, a region exposed to the solvent where amino acids with polar side groups are located to interact with the natural polysaccharide substrate. The hydrophilic portions of these residues are desolvated when the complex with carborane is formed and the system is globally destabilized (Fig. S5, see for example Glu35, Asp52, Arg61). This term takes also into account the desolvation penalty of polar atoms (N—H of Trp63 or C═O of Ala 107) involved in hydrogen/dihydrogen bonding (Fig. S4) with the carborane.

To further validate the MM-GBSA result, a benchmarking procedure was carried out by performing QM/MM calculations (Fig. S6) on 10 structures sampled from the molecular dynamics simulation. The QM/MM interaction energy between the carborane and the protein is −15.2 kcal mol^{-1}, a value fully comparable to the −16.8 kcal mol^{-1} obtained at the MM-GBSA level.

To determine the details of the binding process at the atomic level, we performed a "fingerprint analysis" to quantify the interaction of each amino acid with the carborane. Fig. 4 emphasizes the role of most interacting residues in the binding process.

Dispersion interactions between the indole groups of the tryptophan residues (Trp62, Trp63, and Trp108) and the carborane cage (mediated by C–H···π and B–H···π contacts) [11,12], together with hydrophobic interactions involving the aliphatic side chains of Ile58 and Ile98, are among the most stabilizing contributions to the binding. These interactions create an ideal hydrophobic binding site that accommodates the carborane, as shown in Fig. 4B.

A hydrogen bonding network is observed upon carborane binding and conserved along the MD simulation (Fig. 5 and Fig. S7). Interestingly, both "classical hydrogen bond" and "dihydrogen bonds" [43,44] are observed. In fact, the two acidic C—H bonds of the carborane interact with the carbonyl group of Ala107, while the hydridic B—H bonds engage interactions with the two N$^{\varepsilon}$-H groups of Trp63 and Trp108 and with the peptide N—H bond of Asn59.

It is also noteworthy to underline the existing destabilizing

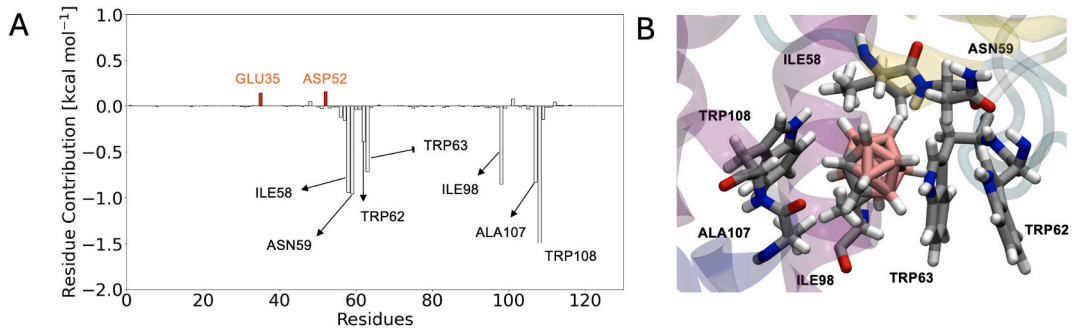

Fig. 4. Carborane@LSZ interactions. A) $E_{binding}$ decomposed per residue.B) Structural representation of the interaction between Ile 58, Trp62, Trp63, Ile 98, Trp108 and carborane.

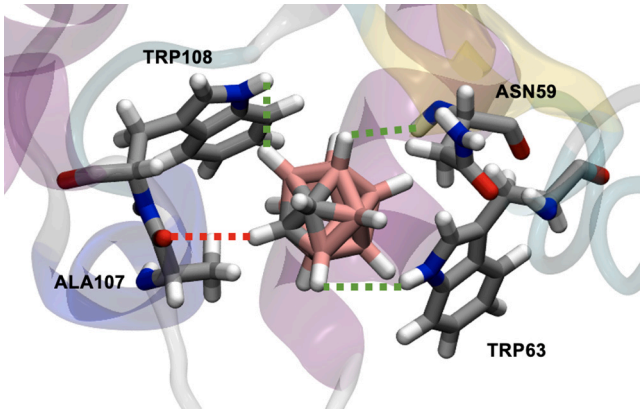

Fig. 5. Hydrogen bond network formed by the carborane upon binding to the lysozyme. In red "classical hydrogen bonds", in green "dihydrogen bonds".

interactions of carborane with Glu35 and Asp52 (the catalytic residues of lysozyme): the molecular electrostatic potential of the carborane is dominated by the hydridic B—H, that are negatively charged, so repulsive electrostatic interactions are observed with the carboxylates of these two residues. These repulsive interactions are directly responsible for the chemical shift perturbations, observed in the NMR experiments, of the Phe34 and Thr51, linked with their peptide bonds to Glu35 and Asp52 and probably of a pushing effect on Thr69 (Fig. S8).

To improve the understanding of the dual nature of carborane, namely, its hydrophobic 3D cage and its ability to form both hydrogen and dihydrogen bonds, and how these features influence its binding preference and selectivity, we performed two additional MD simulations of lysozyme in complex with the isosteric adamantane (3D hydrophobicity) and benzene (2D hydrophobicity) [8]. These compounds are purely hydrophobic and cannot form hydrogen bonds. The results indicate (Figs. S9 and S10) that the 3D hydrophobic structure of carborane is crucial for binding: benzene rapidly leaves the binding site during the MD simulations, whereas adamantane exhibits a binding energy very similar to that of carborane (-18.2 kcal mol^{-1} *vs* -16.8 kcal mol^{-1}) and interacts with the same hydrophobic/aromatic residues (Ile58, Trp63, Ile98, Ala107, Trp108). Interestingly, Asn59 also interacts with both compounds; however, while it engages in a dihydrogen bond with carborane, in the case of adamantane it contacts the aliphatic portion of the side chain through hydrophobic interactions.

Although carborane can form hydrogen and dihydrogen bonds ($E_{el} = -6.1$ kcal mol^{-1}), the associated desolvation penalty (10.0 kcal mol^{-1}) outweighs the stabilizing contribution of these interactions. Consequently, the binding is primarily governed by hydrophobic forces, as demonstrated by the behaviour of adamantane in the simulations: despite lacking any capacity for hydrogen bonding, adamantane binds with an energy comparable to that of carborane and engages the same hydrophobic and aromatic residues within the pocket.

This region of LSZ also constitutes the binding site for several hydrophobic dyes, including ANS (1-anilino-8-naphthalenesulfonate), Hoechst, and azo dyes, whose association is largely driven by hydrophobic interactions [81,82].

The spectroscopic evidence that carborane binds in proximity of the catalytic site of LSZ prompted us to investigate the possible effects of such an interaction on the enzyme catalysis. LSZ catalyses the hydrolysis of the β-1,4-glycosidic bonds in peptidoglycan, the main structural component of the bacterial cell wall, thus leading to bacterial lysis. The activities of free LSZ and carborane@LSZ were determined by turbidimetry (optical density at 450 nm, OD_{450}, see SI for details), namely by monitoring the integrity of *Micrococcus lysodeikticus* over time in the presence of the enzyme.

The carborane@LSZ loses *ca.* 33 % of its catalytic activity, when compared to the free enzyme (Fig. 6A), after ten minutes. These results are consistent with the NMR and MD studies in indicating the interaction of carborane with the enzyme active site pocket. The substrate binding pocket of LSZ consists of a cleft made up of six subsites that accommodate six consecutive sugar moieties of the peptidoglycan chain. Carborane binds to one of these subsites (Fig. 6B), partially clogging the binding pocket and hindering natural substrate access. However, due to its small size, carborane is unable to fully inhibit the enzyme activity.

Carborane binds to LSZ, and its insolubility in water may affect the equilibrium between the bound and free inhibitor. Under such conditions (tight-binding inhibition), and within the framework of classical Michaelis–Menten theory, its kinetic behaviour may resemble that of mixed or noncompetitive inhibitors [83]. To investigate whether this occurs, we measured LSZ activity in the presence and absence of carborane across a range of substrate concentrations using a standard fluorimetric assay, in which 4-methylumbelliferone (4-MU) is released from the substrate 4-methylumbelliferyl β-D-N,N′,N″-triacetylchitotrioside hydrate (NAG_3-MUF).

Considering that the inhibition studies yielded kinetic profiles consistent with mixed or noncompetitive inhibition (Fig. S11), and that NMR data showed that carborane binds within the substrate-binding site, these findings support the interpretation that carborane may inhibit lysozyme activity by binding strongly within the substrate-binding site.

To assess whether our experimental approach could be extended to other proteins, we selected a second model system, bovine serum albumin (BSA). As before, the adduct was obtained through ultrasonication in a heterogeneous phase, followed by purification. The BSA concentration in the complex was measured using UV–visible spectroscopy (Fig. S12), while the carborane content was quantified by MP-AES (Fig. S1B). The resulting molar ratio of carborane to BSA, 2.7 ± 0.5, is consistent with the formation of a stable 3:1 carborane@BSA complex. This value aligns with expectations, as BSA contains multiple binding sites for hydrophobic compounds (namely, seven fatty acid FA binding sites and a cleft binding site). AFM images (Fig. S13) confirmed the

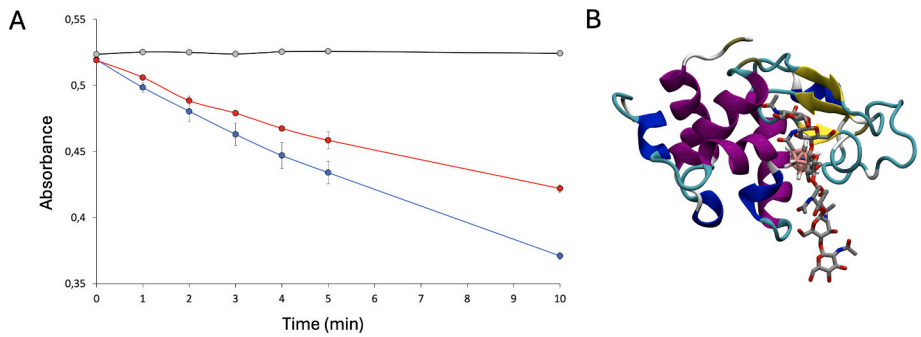

Fig. 6. A) Lysis of *Micrococcus lysodeikticus* cell suspension by LSZ (blue line), carborane@LSZ (red line), control (in the absence of enzyme, gray line). B) Binding of carborane in the LSZ substrate binding pocket. Superposition of carborane with the NAG_6 lysozyme substrate analogue (PDB = 1SFG). (For interpretation of the references to colour in this figure legend, the reader is referred to the web version of this article.)

absence of aggregate formation. Docking calculations identified the three most probable carborane binding sites in BSA: FA5, FA7, and the cleft binding site (Fig. 7). These pockets were further characterized by MD simulations followed by MM-GBSA calculations. The binding affinity of carborane for the three BSA binding pockets (Fig. S14) was even higher than that calculated for LSZ ($E_{binding}$ FA5 = −21.7 kcal mol^{-1}; $E_{binding}$ FA7 = −20.6 kcal mol^{-1}; $E_{binding}$ Cleft = −18.3 kcal mol^{-1}). The trend of the various binding-energy components in the three BSA pockets is very similar among them and closely resembles that of LSZ.

The FA5 binding site is entirely hydrophobic. The most stabilizing contributions arise from dispersion interactions between the benzyl groups of the phenylalanine residues (Phe501 and Phe550) and the carborane cage, along with hydrophobic contacts involving the aliphatic side chains of Ala527, Leu532, and Ala575. The FA7 binding site, in addition to hydrophobic interactions with Leu218, Leu237, Leu289, and Ala290, features also dihydrogen bonds between carborane and Arg217. The cleft binding site is likewise purely hydrophobic. In addition to Ala209, Leu356, Leu480, and Ala481, Lys350 also interacts with the carborane cage through its hydrophobic aliphatic chain, engaging in a surfactant-like interaction. The same key interactions observed with LSZ are also present in BSA.

4. Conclusions

This study presents the first detailed characterization of the interaction between a pristine *closo*-carborane and a model protein (lysozyme) in aqueous solution, shedding light on the molecular determinants that govern carborane-protein recognition process. Using a multidisciplinary approach that combines NMR spectroscopy, AFM imaging, MD simulations, and MM-GBSA binding energy analysis, we demonstrate that carborane selectively binds to a pre-formed hydrophobic cavity in the substrate-binding cleft of LSZ without significantly altering its secondary or tertiary structure.

Binding is dominated by van der Waals and hydrophobic interactions, supported by dispersion forces mediated by C–H···π and B–H···π contacts, with additional stabilization arising from hydrogen-bonding and dihydrogen-bonding contributions. Key interacting residues include aromatic residues and aliphatic side chains, which create a snug hydrophobic pocket ideally suited to accommodate the carborane cage. Despite partial activity inhibition due to obstruction of the active site, the enzyme retains most of its functionality, suggesting that the size of carborane and interaction mode allow for modulated interference rather than full blockage. Kinetic studies are consistent with carborane behaving as a tight-binding competitive inhibitor. These findings highlight the capability of carborane to engage in selective, non-disruptive

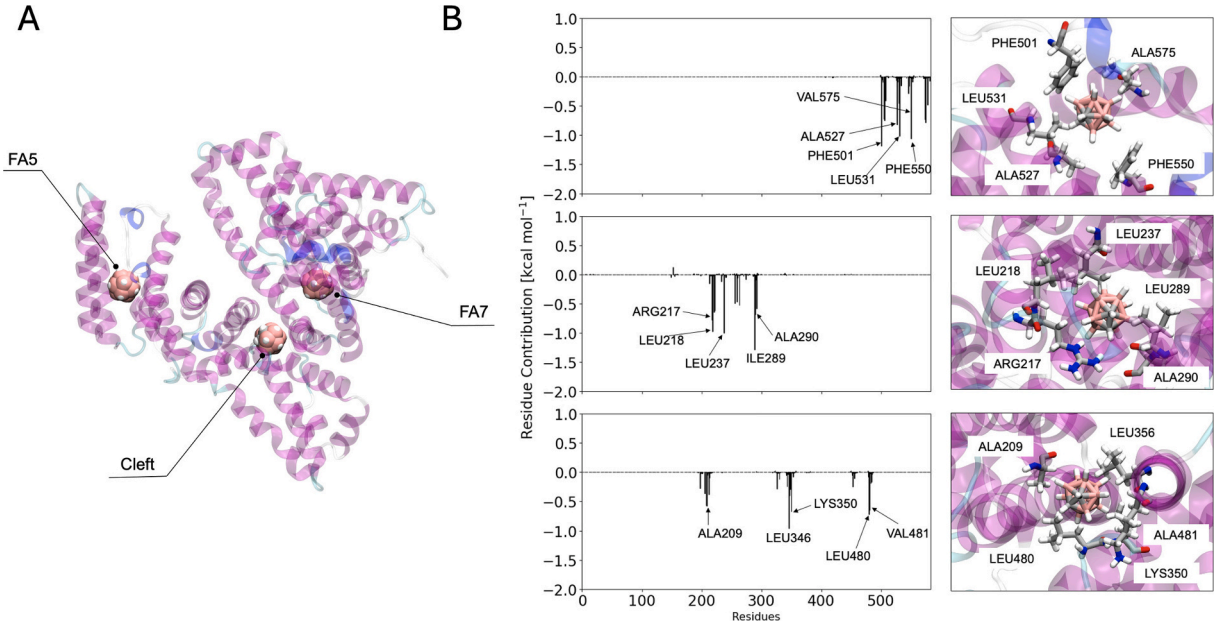

Fig. 7. A) Most probable carborane-binding sites in BSA. B) Fingerprint analysis and 3D representation of the interactions between carborane and BSA in the FA5 binding pocket (top), FA7 binding site (middle), and cleft region (bottom).

protein interactions through its unique chemical features.

By applying our experimental approach to a second model protein, BSA, we demonstrated its broader applicability. The shared characteristics of the binding sites in both proteins suggest common features in the supramolecular binding of carborane to proteins. The implications extend beyond drug development to areas such as protein tagging, delivery strategies for BNCT, and the rational design of carborane-based inhibitors. The ability of proteins to disperse carborane opens promising opportunities for its application in nanomedicine, especially through the design of theranostic and multimodal protein-based nanoparticles. Importantly, this work establishes a foundational framework for future studies aimed at exploiting pristine carboranes as versatile bioactive components in medicinal and structural biology.

CRediT authorship contribution statement

Tainah Dorina Marforio: Writing – original draft, Methodology, Investigation, Formal analysis, Data curation. **Andrea Carboni:** Writing – original draft, Investigation, Formal analysis, Data curation. **Luca Mazzei:** Writing – original draft, Investigation, Formal analysis, Data curation. **Sara Cascone:** Investigation. **Lorenzo Lovatti:** Investigation. **Edoardo Jun Mattioli:** Investigation, Formal analysis. **Francesco Valle:** Methodology, Investigation, Formal analysis. **Matteo Di Giosia:** Investigation, Formal analysis. **Stefano Ciurli:** Writing – original draft, Supervision, Methodology, Investigation, Formal analysis, Data curation. **Matteo Calvaresi:** Writing – review & editing, Writing – original draft, Supervision, Methodology, Investigation, Funding acquisition, Formal analysis, Conceptualization.

Declaration of competing interest

The authors declare that they have no known competing financial interests or personal relationships that could have appeared to influence the work reported in this paper.

Acknowledgements

T.D.M. was supported by a FIRC-AIRC fellowship for Italy (ID. 25554). T.D.M and E.J.M were supported by Fondazione Umberto Veronesi. T.D.M. acknowledges PRACE for awarding access to the Fenix Infrastructure resources, which are partially funded from the European Union's Horizon 2020 research and innovation programme through the ICEI project under the grant agreement No. 800858. S.C. and L.M. acknowledge the Consorzio Interuniversitario di Risonanze Magnetiche di Metallo-Proteine (CIRMMP) for granting access to the European large scale NMR facility at the Center for Magnetic Resonance (CERM – University of Florence, Italy).

Appendix A. Supplementary data

Supplementary data to this article can be found online at https://doi.org/10.1016/j.jcis.2025.139798.

Data availability

Data will be made available on request.

References

[1] M. Schoz, E. Hey-Hawkins, Carbaboranes as pharmacophores: properties, synthesis, and application strategies, Chem. Rev. 111 (2011) 7035–7062.
[2] R. Núñez, M. Tarrés, A. Ferrer-Ugalde, F.F. De Biani, F. Teixidor, Electrochemistry and photoluminescence of icosahedral Carboranes, boranes, Metallacarboranes, and their derivatives, Chem. Rev. 116 (2016) 14307–14378.
[3] Y. Chen, F. Du, L. Tang, J. Xu, Y. Zhao, X. Wu, M. Li, J. Shen, Q. Wen, C.H. Cho, Z. Xiao, Carboranes as unique pharmacophores in antitumor medicinal chemistry, Molecular Therapy: Oncolytics 24 (2022) 400–416.
[4] J.F. Valliant, K.J. Guenther, A.S. King, P. Morel, P. Schaffer, O.O. Sogbein, K. A. Stephenson, The medicinal chemistry of carboranes, Coord. Chem. Rev. 232 (2002) 173–230.
[5] A.F. Armstrong, J.F. Valliant, The bioinorganic and medicinal chemistry of carboranes: from new drug discovery to molecular imaging and therapy, Dalton Trans. 38 (2007) 4240–4251.
[6] Z.O. Emilia, M.A. Christian, J. Mark, W. Lee, The use of Carboranes in Cancer drug development, Int. J. Cancer Clin. Res. 6 (2019) 110.
[7] A. Marfavi, P. Kavianpour, L.M. Rendina, Carboranes in drug discovery, chemical biology and molecular imaging, Nat. Rev. Chem. 6 (2022) 486–504.
[8] F. Issa, M. Kassiou, L.M. Rendina, Boron in drug discovery: Carboranes as unique pharmacophores in biologically active compounds, Chem. Rev. 111 (2011) 5701–5722.
[9] P. Stockmann, M. Gozzi, R. Kuhnert, M.B. Sárosi, E. Hey-Hawkins, New keys for old locks: carborane-containing drugs as platforms for mechanism-based therapies, Chem. Soc. Rev. 48 (2019) 3497–3512.
[10] T.D. Marforio, A. Carboni, M. Calvaresi, In vivo application of Carboranes for boron neutron capture therapy (BNCT): structure, Formulation and Analytical Methods for Detection, Cancers 15 (2023) 4944.
[11] J. Fanfrlík, J. Brynda, M. Kugler, M. Lepšík, K. Pospíšilová, J. Holub, D. Hnyk, J. Nekvinda, B. Grüner, P. Řezáčová, B–H···π and C–H···π interactions in protein–ligand complexes: carbonic anhydrase II inhibition by carborane sulfonamides, Phys. Chem. Chen. Phys., 25 (2023), 1728–1733.
[12] J. Fanfrlík, A. Pecina, J. Řezáč, R. Sedlak, D. Hnyk, M. Lepšík, P. Hobza, B–H···π: a nonclassical hydrogen bond or dispersion contact? Phys. Chem. Chen. Phys. 19 (2017) 18194–18200.
[13] M. Calvaresi, F. Zerbetto, In silico Carborane docking to proteins and potential drug targets, J. Chem. Inf. Model. 51 (2011) 1882–189614.
[14] P. Mader, A. Pecina, P. Cígler, M. Lepšík, V. Šícha, P. Hobza, B. Grüner, J. Fanfrlík, J. Brynd, P. Řezáčová, Carborane-based carbonic anhydrase inhibitors: insight into CAII/CAIX specificity from a high-resolution crystal structure, Modeling, and quantum chemical calculations, Biomed. Res. Int. 1 (2014) 389869.
[15] M. Kugler, J. Holub, J. Brynda, K. Pospíšilová, S. El Anwar, D. Bavol, M. Havránek, V. Král, M. Fábry, B. Grüner, P. Řezáčová, The structural basis for the selectivity of sulfonamido dicarbaboranes toward cancer-associated carbonic anhydrase IX, J. Enzyme Inhib. Med. Chem. 35 (2020) 1800–1810.
[16] P. Řezáčová, J. Pokorná, J. Brynda, M. Kožíšek, P. Cígler, M. Lepšík, J. Fanfrlík, J. Řezáč, K.G. Šašková, I. Sieglová, J. Plešek, V. Šícha, B. Grüner, H. Oberwinkler, J. Sedláček', H. G. Kräusslich, P. Hobza, V. Král, J. Konvalink, Design of HIV Protease Inhibitors Based on Inorganic Polyhedral Metallacarboranes, J. Med. Chem. 52 (2009) 7132–7141.
[17] S. Fujii, H. Masuno, Y. Taoda, A. Kano, A. Wongmayura, M. Nakabayashi, N. Ito, M. Shimizu, E. Kawachi, T. Hirano, Y. Endo, A. Tanatani, H. Kagechika, Boron cluster-based development of potent Nonsecosteroidal vitamin D receptor ligands: direct observation of hydrophobic interaction between protein surface and Carborane, J. Am. Chem. Soc. 133 (2011) 20933–20941.
[18] F. Heide, M. McDougall, C. Harder-Viddal, R. Roshko, D. Davidson, J. Wu, C. Aprosoff, A. Moya-Torres, F. Lin, J. Stetefeld, Boron rich nanotube drug carrier system is suited for boron neutron capture therapy, Sci. Rep. 11 (2021) 15520.
[19] R.L. Julius, O.K. Farha, J. Chiang, L.J. Perry, M.F. Hawthorne, Synthesis and evaluation of transthyretin amyloidosis inhibitors containing carborane pharmacophores, Proc. Nat. Acad. Sci. 104 (2007) 4808–4813.
[20] B. Grüner, M. Kugler, S. El Anwar, J. Holub, J. Nekvinda, D. Bavol, Z. Růžičková, K. Pospíšilová, M. Fábry, V. Král, J. Brynda, P. Řezáčová, Cobalt bis(dicarbollide) Alkylsulfonamides: potent and highly selective inhibitors of tumor specific carbonic anhydrase IX, ChemPlusChem 86 (2021) 352–363.
[21] J. Nekvinda, M. Kugler, J. Holub, S. El Anwar, J. Brynda, K. Pospíšilová, Z. Růžičková, P. Řezáčová, B. Grüner, Direct introduction of an Alkylsulfonamido group on C-sites of isomeric Dicarba-closo-dodecaboranes: the influence of stereochemistry on inhibitory activity against the Cancer-associated carbonic anhydrase IX isoenzyme, Chem. A Eur. J. 26 (2020) 16541–16553.
[22] R. Otero, S. Seoane, R. Sigüeiro, A.Y. Belorusova, M.A. Maestro, R. Pérez-Fernández, N. Rochel, A. Mouriño, Carborane-based design of a potent vitamin D receptor agonist, Chem. Sci. 7 (2016) 1033–1037.
[23] J. Dvořanová, M. Kugler, J. Holub, V. Šícha, V. Das, J. Nekvinda, S. El Anwar, M. Havránek, K. Pospíšilová, M. Fábry, V. Král, M. Medvedíková, S. Matějková, B. Lišková, S. Gurská, P. Džubák, J. Brynda, M. Hajdúch, B. Grüner, P. Řezáčová, Sulfonamido carboranes as highly selective inhibitors of cancer-specific carbonic anhydrase IX, Eur. J. Med. Chem. 200 (2020) 112460.
[24] J. Brynda, P. Mader, V. Šícha, M. Fábry, K. Poncová, M. Bakardiev, B. Grüner, P. Cígler, P. Řezáčová, Carborane-based carbonic anhydrase inhibitors, Angew. Chem. – Inter. Ed. 52 (2013) 13760–13763.
[25] M. Kožíšek, P. Cígler, M. Lepšík, J. Fanfrlík, P. Řezáčová, J. Brynda, J. Pokorná, J. Plešek, B. Grüner, K.G. Šašková, J. Václavíková, V. Král, J. Konvalinka, Inorganic polyhedral Metallacarborane inhibitors of HIV protease: a new approach to overcoming antiviral resistance, J. Med. Chem. 51 (2008) 4839–4843.
[26] P. Cígler, M. Kozísek, P. Rezácová, J. Brynda, Z. Otwinowski, J. Pokorná, J. Plesek, B. Grüner, L. Dolecková-Maresová, M. Másа, J. Sedlácek, J. Bodem, H. G. Kräusslich, V. Král, J. Konvalinka, From nonpeptide toward noncarbon protease inhibitors: metallacarboranes as specific and potent inhibitors of HIV protease, Proc. Nat. Acad. Sci. 102 (2005) 15394–15399.
[27] E.L. Crossley, F. Issa, A.M. Scarf, M. Kassiou, L.M. Rendina, Synthesis and cellular uptake of boron-rich pyrazolopyrimidines: exploitation of the translocator protein for the efficient delivery of boron into human glioma cells, Chem. Commun. 47 (2011) 12179–12181.

[28] R.C. Reynolds, S.R. Campbell, R.G. Fairchild, R.L. Kisliuk, P.L. Micca, S.F. Queener, J.M. Riordan, W.D. Sedwick, W.R. Waud, A.K.W. Leung, R.W. Dixon, W.J. Suling, D.W. Borhani, Novel boron-containing, nonclassical antifolates: synthesis and preliminary biological and structural evaluation, J. Med. Chem. 50 (2007) 3283–3289.

[29] Y. Shao, K. Miura, Y. Asawa, T. Morita, G. Li, H. Nakamura, Discovery of disubstituted Carboranes as inhibitors of heat shock protein 90–heat shock factor 1 interaction, ACS Med. Chem. Lett. 15 (2024) 619–625.

[30] L. Kuhnert, R. Kuhnert, M.B. Sárosi, C. Lakoma, B.K. Scholz, P. Lönnecke, E. Hey-Hawkins, W. Honscha, Enhanced reversal of ABCG2-mediated drug resistance by replacing a phenyl ring in baicalein with a meta-carborane, Mol. Oncol. 18 (2024) 280–290.

[31] D. Sedlák, T.A. Wilson, W. Tjarks, H.S. Radomska, H. Wang, J.N. Kolla, Z. J. Leśnikowski, A. Špičáková, T. Ali, K. Ishita, L.H. Rakotondraibe, S. Vibhute, D. Wang, P. Anzenbacher, C. Bennett, P. Bartunek, C.C. Coss, Structure-activity relationship of Para-Carborane selective Estrogen receptor β agonists, J. Med. Chem. 64 (2021) 9330–9353.

[32] M. Kugler, J. Nekvinda, J. Holub, S. El Anwar, V. Das, V. Šícha, K. Pospíšilová, M. Fábry, V. Král, J. Brynda, V. Kašička, M. Hajdúch, P. Řezáčová, B. Grüner, Inhibitors of CA IX enzyme based on polyhedral boron compounds, ChemBioChem 22 (2021) 2241–2761.

[33] C. Selg, A. Schöler, J. Schliehe-Diecks, M. Hanl, L. Sinatra, A. Borkhardt, M. B. Sárosi, S. Bhatia, E. Hey-Hawkins, F.K. Hansen, Borinostats: solid-phase synthesis of carborane-capped histone deacetylase inhibitors with a tailor-made selectivity profile, Chem. Sci. 12 (2021) 11873–11881.

[34] C. Alamón, B. Dávila, M.F. García, C. Sánchez, M. Kovacs, E. Trias, L. Barbeito, M. Gabay, N. Zeineh, M. Gavish, F. Teixidor, C. Viñas, M. Couto, H. Cerecetto, Sunitinib-containing Carborane pharmacophore with the ability to inhibit tyrosine kinases receptors FLT3, KIT and PDGFR-β, Exhibits Powerful In Vivo Anti-Glioblastoma Activity, Cancers 12 (2020) 3423.

[35] R. Kuhnert, M.B. Sárosi, S. George, P. Lönnecke, B. Hofmann, D. Steinhilber, B. Murganic, S. Mijatovic, D. Maksimovic-Ivanic, E. Hey-Hawkins, CarbORev-5901: the first Carborane-based inhibitor of the 5-lipoxygenase pathway, ChemMedChem 12 (2017) 1081–1086.

[36] S. Fujii, T. Goto, K. Ohta, Y. Hashimoto, T. Suzuki, S. Ohta, Y. Endo, Potent androgen antagonists based on Carborane as a hydrophobic Core structure, J. Med. Chem. 48 (2005) 4654–4662.

[37] K. Ohta, T. Iijima, E. Kawachi, H. Kagechika, Y. Endo, Novel retinoid X receptor (RXR) antagonists having a dicarba-closo-dodecaborane as a hydrophobic moiety, Bioorg. Med. Chem. Lett. 14 (2004) 5913–5918.

[38] K. Fink, M. Uchman, Boron cluster compounds as new chemical leads for antimicrobial therapy, Coord. Chem. Rev. 431 (2021) 213684.

[39] T.J.C. Carraro, S. Dasgupta, J. Ku, S.R. Thomas, L.M. Rendina, Boron-based functionalities enhance, the potency of 2,5-dimethylfuran-based IDO1 inhibitors, ChemBioChem 26 (2025) e202500134.

[40] N. Smith, D. Quan, G. Nagalingam, J.A. Triccas, L.M. Rendina, P.J. Rutledge, Carborane clusters increase the potency of bis-substituted cyclam derivatives against mycobacterium tuberculosis, RSC Med Chem 13 (2022) 1234–1238.

[41] P. Kavianpour, M.C.M. Gemmell, J.U. Kahlert, L.M. Rendina, Histone deacetylase 2 (HDAC2) inhibitors containing boron, ChemBioChem 21 (2020) 2786–2791.

[42] Y. Asawa, K. Nishida, K. Kawai, K. Domae, H.S. Ban, A. Kitazaki, H. Asami, J. Y. Kohno, S. Okada, H. Tokuma, D. Sakano, S. Kume, M. Tanaka, H. Nakamura, Carborane as an alternative efficient hydrophobic tag for protein degradation, Bioconjug. Chem. 32 (2021) 2377–2385.

[43] J. Fanfrlík, M. Lepšík, D. Horinek, Z. Havlas, P. Hobza, Interaction of Carboranes with biomolecules: formation of dihydrogen bonds, ChemPhysChem 7 (2006) 1100–1105.

[44] A. Pecina, M. Lepšik, J. Rezac, J. Brynda, P. Mader, P. Řezáčová, P. Hobza, J. Fanfrlík, QM/MM calculations reveal the different nature of the interaction of two Carborane-based Sulfamide inhibitors of human carbonic anhydrase II, J. Phys. Chem. 117 (2013) 16096–16104.

[45] M. Di Giosia, F. Zerbetto, M. Calvaresi, Incorporation of molecular nanoparticles inside proteins: the trojan horse approach in Theranostics, Acc. Mater. Res. 2 (2021) 594–605.

[46] T.D. Marforio, E.J. Mattioli, F. Zerbetto, M. Calvaresi, Exploiting blood transport proteins as Carborane supramolecular vehicles for boron neutron capture therapy, Nanomaterials 13 (2023) 1770.

[47] T.M. Goszczyński, K. Fink, K. Kowalski, Z.J. Leśnikowski, J. Boratyński, Interactions of boron clusters and their derivatives with serum albumin, Sci. Rep. 7 (2017) 1–12.

[48] J. Zhang, Q. Zhang, X. Li, Y. Wei, M. Qiu, H. Yang, X. Sun, Prominent supramolecular systems for cancer therapy: from structural design to tailored applications, Eur. J. Med. Chem. 294 (2025) 117754.

[49] G. Moreno-Alcántar, M. Drexler, A. Casini, Assembling a new generation of radiopharmaceuticals with supramolecular theranostics, Nat. Rev. Chem. 8 (2024) 893–914.

[50] S. Li, Y. Wang, C. Li, B. Zhou, X. Zeng, H. Zhu, Supramolecular nanomedicine in the intelligent cancer therapy: recent advances and future, Front. Pharmacol. 15 (2024) 1490139.

[51] T.U. Probst, N.G. Berryman, P. Lemmen, L. Weissfloch, T. Auberger, D. Gabel, J. Carlsson, B. Larsson, Comparison of inductively coupled plasma atomic emission spectrometry and inductively coupled plasma mass spectrometry with quantitative neutron capture radiography for the determination of boron in biological samples from Cancer therapy, J. Anal. At. Spectrom 12 (1997) 1115–1122.

[52] M. He, L. Deng, H. Lud, Z. Jin, Elimination of the boron memory effect for rapid and accurate boron isotope analysis by MC-ICP-MS using NaF, J. Anal. At. Spectrom 34 (2019) 1026–1031.

[53] F. Valle, J.A. DeRose, G. Dietler, M. Kawe, A. Pluckthun, G. Semenza, AFM structural study of the molecular chaperone GroEL and its two-dimensional crystals: an ideal "living" calibration sample, Ultramicroscopy 93 (2002) 83–89.

[54] F. Delaglio, S. Grzesiek, G.W. Vuister, G. Zhu, J. Pfeifer, A. Bax, NMRPipe: a multidimensional spectral processing system based on UNIX pipes, J. Biomol. NMR 6 (1995) 277–293.

[55] J. Ying, C.A. Barnes, J.M. Louis, A. Bax, Importance of time-ordered non-uniform sampling of multi-dimensional NMR spectra of $A\beta^{1-42}$ peptide under aggregating conditions, J. Biomol. NMR 73 (2019) 429–441.

[56] W. Lee, M.M. Rahimi, Y. Lee, A. Chiu, POKY: a software suite for multidimensional NMR and 3D structure calculation of biomolecules, Bioinformatics 37 (2021) 3041–3042.

[57] M.P. Williamson, Using chemical shift perturbation to characterise ligand binding, Prog. Nucl. Magn. Reson. Spectrosc. 73 (2013) 1–16.

[58] R.A. Williamson, M.D. Carr, T.A. Frenkiel, J. Feeney, R.B. Freedman, Mapping the binding site for matrix metalloproteinase on the N-terminal domain of the tissue inhibitor of metalloproteinases-2 by NMR chemical shift perturbation, Biochemistry 36 (1997) 13882–13889.

[59] Sigma-Aldrich, "Enzymatic assay of lysozyme",https://www.sigmaaldrich.com/IT/it/technical-documents/protocol/protein-biology/enzyme-activity-assays/enzymatic-assay-of-lysozyme?srsltid=AfmBOooKw6bSV8RPK2sBsUzABnqr8OsGIpLKED5EATn8jl68qdK2g3x4.

[60] J.C. Cheetham, P.J. Artymiuk, D.C. Phillips, Refinement of an enzyme complex with inhibitor bound at partial occupancy. Hen egg-white lysozyme and tri-N-acetylchitotriose at 1.75 a resolution, J. Mol. Biol. 224 (1992) 613–628.

[61] A. Bujacz, Structures of bovine, equine and leporine serum albumin, *acta Cryst.,* D68 (2012),1278–1289.

[62] D. Schneidman-Duhovny, Y. Inbar, V. Polak, M. Shatsky, I. Halperin, H. Benyamini, A. Barzilai, O. Dror, N. Haspel, R. Nussinov, Taking geometry to its edge: fast unbound rigid (and hinge-bent) docking, Proteins Struct. Funct. Genet. 52 (2003) 107–112.

[63] J. Wang, J.W. Wolf, P.A. Caldwell, D.A. Kollman, Case, development and testing of a general amber force field, J. Comput. Chem. 25 (2004) 1157–1174.

[64] M.B. Sàrosi, T.P. Lybrand, Molecular dynamics simulation of Cyclooxygenase-2 complexes with indomethacin closo-Carborane Analog, J. Chem. Inf. Model. 58 (2018), 1990–199.

[65] D. A. Case, R.M. Betz, D.S. Cerutti, T.E. Cheatham, III, T.A. Darden, R.E. Duke, T.J. Giese, H. Gohlke, A.W. Goetz, N. Homeyer, S. Izadi, P. Janowski, J. Kaus, A. Kovalenko, T.S. Lee, S. LeGrand, P. Li, C. Lin, T. Luchko, R. Luo, B. Madej, D. Mermelstein, K.M. Merz, G. Monard, H. Nguyen, H.T. Nguyen, I. Omelyan, A. Onufriev, D.R. Roe, A. Roitberg, *C. sagui*, C.L. Simmerling, W.M. Botello-Smith, J. Swails, R.C. Walker, J. Wang, R.M. Wolf, X. Wu, L. Xiao, P.A. Kollman, AMBER16 (2016), University of California, San Francisco.

[66] D.R. Roe, T.E. Cheatham, PTRAJ and CPPTRAJ: software for processing and analysis of molecular dynamics trajectory data, J. Chem. Theory Comput. 9 (2013) 3084–3095.

[67] G.D. Hawkins, C.J. Cramer, D.J. Truhlar, Pairwise solute descreening of solute charges from a dielectric medium *chem*, Phys. Lett. 246 (1995) 122–129.

[68] G.D. Hawkins, C.J. Cramer, D.G. Truhlar, Parametrized models of aqueous free energies of solvation based on pairwise Descreening of solute atomic charges from a dielectric medium, J. Phys. Chem. 100 (1996) 19824–19839.

[69] T. Vreven, K.S. Byun, I. Komáromi, S. Dapprich, J.A. Montgomery, K. Morokuma, M.J. Frisch, Combining quantum mechanics methods with molecular mechanics methods in ONIOM, J. Chem. Theory Comput. 2 (2006) 815–826.

[70] S. Dapprich, I. Komaromi, K. Suzie Byun, K. Morokuma, M. J. Frisch, A new ONIOM implementation in Gaussian98. Part I. The calculation of energies, gradients, vibrational frequencies and electric field derivatives, *J. Mol. Struct.: THEOCHEM,* 461–462 (1999), 1–21.

[71] M. J. Frisch, G. W. Trucks, H. B. Schlegel, G. E. Scuseria, M. A. Robb, J. R. Cheeseman, G. Scalmani, V. Barone, G. A. Petersson, H. Nakatsuji, X. Li, M. Caricato, A. V. Marenich, J. Bloino, B. G. Janesko, R. Gomperts, B. Mennucci, H. P. Hratchian, J. V. Ortiz, A. F. Izmaylov, J. L. Sonnenberg, D. Williams-Young, F. Ding, F. Lipparini, F. Egidi, J. Goings, B. Peng, A. Petrone, T. Henderson, D. Ranasinghe, V. G. Zakrzewski, J. Gao, N. Rega, G. Zheng, W. Liang, M. Hada, M. Ehara, K. Toyota, R. Fukuda, J. Hasegawa, M. Ishida, T. Nakajima, Y. Honda, O. Kitao, H. Nakai, T. Vreven, K. Throssell, J. A. Montgomery, Jr., J. E. Peralta, F. Ogliaro, M. J. Bearpark, J. J. Heyd, E. N. Brothers, K. N. Kudin, V. N. Staroverov, T. A. Keith, R. Kobayashi, J. Normand, K. Raghavachari, A. P. Rendell, J. C. Burant, S. S. Iyengar, J. Tomasi, M. Cossi, J. M. Millam, M. Klene, C. Adamo, R. Cammi, J. W. Ochterski, R. L. Martin, K. Morokuma, O. Farkas, J. B. Foresman, and D. J. Fox, Gaussian, Inc., Wallingford CT, 2016.L.

[72] W. Chung, W.M.C. Sameera, R. Ramozzi, A.J. Page, M. Hatanaka, G.P. Petrova, T. V. Harris, X. Li, Z. Ke, F. Liu, H.B. Li, L. Ding, K. Morokuma, The ONIOM method and its applications, Chem. Rev. 115 (2015) 5678–5796.

[73] M. Calvaresi, F. Arnesano, S. Bonacchi, A. Bottoni, V. Calò, S. Conte, G. Falini, S. Fermani, M. Losacco, M. Montalti, G. Natile, L. Prodi, F. Sparla, F. Zerbetto, C60@lysozyme: direct observation by nuclear magnetic resonance of a 1:1 fullerene protein adduct, ACS Nano 8 (2014) 1871–1877.

[74] M. Di Giosia, A. Soldà, M. Seeger, A. Cantelli, F. Arnesano, M.I. Nardella, V. Mangini, F. Valle, M. Montalti, F. Zerbetto, S. Rapino, M. Calvaresi, V. Ntziachristos, A bio-conjugated fullerene as a subcellular-targeted and multifaceted Phototheranostic agent, Adv. Funct. Mater. 31 (2021) 2101527.

[75] M. Di Giosia, P.H.H. Bomans, A. Bottoni, A. Cantelli, G. Falini, P. Franchi, G. Guarracino, H. Friedrich, M. Lucarini, F. Paolucci, S. Rapino, N.A.J. M. Sommerdijk, A. Soldà, F. Valle, F. Zerbetto, M. Calvaresi, Proteins as supramolecular hosts for C60: a true solution of C60 in water, Nanoscale 10 (2018) 9908–9916.
[76] M. Berto, M. Di Giosia, M. Giordani, M. Sensi, F. Valle, A. Alessandrini, C. Menozzi, A. Cantelli, G.C. Gazzadi, F. Zerbetto, F. Biscarini, C.A. Bortolotti, Green fabrication of (6,5)carbon nanotube/protein transistor endowed with specific recognition, Adv. Electron. Mater. 7 (2021) 2001114.
[77] J. Neburkova, A.M. Rulseh, S.L.Y. Chang, H. Raabova, J. Vejpravova, M. Dracinsky, J. Tarabek, J. Kotek, M. Pingle, P. Majer, J. Vymazal, P. Cigler, Formation of gadolinium–ferritin from clinical magnetic resonance contrast agents, Nanoscale Adv. 2 (2020) 5567–5571.
[78] M. Assfalg, L. Ragona, K. Pagano, M. D'Onofrio, S. Zanzoni, S. Tomaselli, H. Molinari, The study of transient protein–nanoparticle interactions by solution NMR spectroscopy, Biochim. Biophys. Acta 2016 (1864) 102–114.
[79] A. Bortot, S. Zanzoni, M. D'Onofrio, M. Assfalg, Specific interaction sites determine differential adsorption of protein structural isomers on nanoparticle surfaces, Chemistry - Eur. J. 24 (2018) 5911–5919.
[80] E. Chovancova, A. Pavelka, P. Benes, O. Strnad, J. Brezovsky, B. Kozlikova, A. Gora, V. Sustr, M. Klvana, P. Medek, L. Biedermannova, J. Sochor, J. Damborsky, CAVER 3.0: a tool for the analysis of transport pathways in dynamic protein structures, PLoS Comput. Biol. 8 (2012) e1002708.
[81] A. Basu, G.S. Kumar, Interaction and inhibitory influence of the azo dye carmoisine on lysozyme amyloid fibrillogenesis, Mol. Biosyst. 13 (2017) 1552–1564.
[82] P. Mandal, I. Pramanick, D. Shit, S. Pramanik, Unveiling the interaction of hoechst 33258 with lysozyme: a spectroscopic and molecular docking study, J. Mol. Struct. 1355 (2026) 145018.
[83] J. Reis, N. Manzella, F. Cagide, J. Mialet-Perez, E. Uriarte, A. Parini, F. Borges, C. Binda, Tight-binding inhibition of human monoamine oxidase B by chromone Analogs: a kinetic, crystallographic, and biological analysis, J. Med. Chem. 61 (2018) 4203–4212.